Catalysis Today 283 (2017) 119–126

Contents lists available at ScienceDirect

Catalysis Today

journal homepage: www.elsevier.com/locate/cattod

In situ formation of hydrides and carbides in palladium catalyst: When XANES is better than EXAFS and XRD

Aram L. Bugaev[a,b,*], Alexander A. Guda[a], Andrea Lazzarini[b], Kirill A. Lomachenko[a], Elena Groppo[b], Riccardo Pellegrini[c], Andrea Piovano[d], Hermann Emerich[e], Alexander V. Soldatov[a], Lusegen A. Bugaev[a], Vladimir P. Dmitriev[a,e], Jeroen A. van Bokhoven[f,g], Carlo Lamberti[a,h,*]

[a] IRC "Smart Materials", Southern Federal University, Zorge Street 5, 344090 Rostov-on-Don, Russia
[b] Department of Chemistry, NIS and INSTM Reference Centers, University of Torino, via Quarello 15, I-10135 Torino, Italy
[c] Chimet SpA—Catalyst Division, via Di Pescaiola 74, Arezzo, 52041 Italy
[d] Institute Laue-Langevin (ILL), 71 Avenue des Martyrs, 38000 Grenoble, France
[e] SNBL at ESRF, 71 Avenue des Martyrs, 38000 Grenoble, France
[f] Institute for Chemical and Bioengineering, ETH Zurich, HCI E127, 8093 Zurich, Switzerland
[g] Paul Scherrer Institute, 5232 Villigen, Switzerland
[h] Department of Chemistry, CrisDi Centre for Crystallography, University of Torino, via Giuria 7, I-10125 Torino, Italy

ARTICLE INFO

Article history:
Received 21 November 2015
Received in revised form 20 January 2016
Accepted 15 February 2016
Available online 12 April 2016

Keywords:
Palladium hydride
Palladium carbide
EXAFS
XRPD
XANES simulations
Monte Carlo simulations

ABSTRACT

In a number of hydrogenation reactions, palladium nanoparticles may undergo a transition to the hydride or the carbide phase, which affects the catalytic properties. In the current work, we determine the structural evolution of an industrial Pd/C catalyst in the presence of hydrogen and acetylene by means of *in situ* X-ray absorption spectroscopy and X-ray powder diffraction. We observe reversible hydride phase formation and irreversible formation of the carbide phase. The near-edge structure of the absorption spectra (XANES) plays the key role in distinguishing between hydride and carbide phases. We show that the presence of hydrogen and carbon atoms have a direct effect on the near-edge region which is reproduced by theoretical simulations performed in the Monte-Carlo approach.

1. Introduction

Metal nanoparticles play an important role in catalysis [1–13]. In the preparation of catalysts for hydrogenation of hydrocarbons, such as alkynes and alkenes, palladium is recognized as the preferred metal. In reaction conditions, palladium nanoparticles may undergo phase changes to hydride and carbide phases, whose natures affect the catalytic properties [14,15]. Therefore, determining the hydride and carbide formation during a catalytic process becomes an important problem, also relevant to industry. Being a subject of numerous theoretical [16–20] and experimental [19,21–34] studies, palladium hydride is one of the most studied metal hydrides. In contrast to the hydride, the structure and properties of the carbide phase are still under discussion [14,22,24,35,36].

The formation of both hydride and carbide phases is accompanied with an expansion of the palladium lattice, which can be followed by X-ray powder diffraction (XRPD) [37–39] and extended X-ray absorption fine structure (EXAFS) [24,34,36,40,41]. EXAFS is an element-selective technique and demonstrates high sensitivity to the local structure changes, such as bond distances and coordination numbers of the absorbing atom [4,12,13,42–46]. For palladium containing material, whose K-absorption edge is 24357 eV, hard X-rays can be easily applied to perform *in situ* and *operando* experiments [13,45,47–53]. At the same time, XRPD is a phase-selective technique and it gives detailed information on the crystalline phases, which is important if several phases coexist in the sample. In particular, XRPD has been successfully applied to determine the concentrations of α- and β- hydride phases in palladium particles during palladium hydride phase transition [54]. However, this approach is hard to be applied when the nanoparticles are

* Corresponding authors at: IRC "Smart Materials", Southern Federal University, Zorge Street 5, 344090, Rostov-on-Don, Russia.
E-mail addresses: abugaev@sfedu.ru (A.L. Bugaev), carlo.lamberti@unito.it (C. Lamberti).

http://dx.doi.org/10.1016/j.cattod.2016.02.065
0920-5861/

deposited on a crystalline support [34] and for nanoparticles with the size below 1.5 nm [54], where the weak and relatively broad Bragg peaks of the diluted metal phase (typically few wt.%) is overshadowed by the scattering from the dominant support phase. One should take into consideration that both EXAFS and XRPD are least sensitive to light atoms, such as carbon and especially hydrogen, due to their low scattering amplitudes compared to palladium. Thus, palladium hydride and carbide phases are observed by these techniques almost only indirectly, i.e. *via* Pd-Pd distance elongation or lattice expansion.

X-ray absorption near-edge structure (XANES) include a part of the absorption spectrum up to 30–50 eV above the absorption edge [12,13,46,55–58]. K-edge XANES probes the transition of 1s electron to empty np orbitals and is consequently sensitive to changes in the structure of unoccupied electronic states with p-symmetry. It was shown [20,34–36,59,60] that the formation of palladium hydride directly affects the shape of the X-ray absorption near edge structure due to mixing of unoccupied states of hydrogen and palladium. This makes XANES a promising tool for in situ investigation of palladium hydride and carbide formation, because unlike EXAFS and XRPD this method is sensitive to the presence of light atoms [25,61,62].

The aim of the current work is to present a systematic approach for *in situ* and *operando* investigation of the formation of hydride and carbide phases in an industrial palladium-based catalyst under realistic working conditions. We show that simultaneous utilization of XRPD, EXAFS and XANES allows obtaining complementary information on the nanocatalyst structure modification induced by the presence of the reactants. The special role in discriminating between hydride and carbide phases is given to XANES. The changes observed in XANES spectra of the palladium catalyst under reaction conditions are reproduced by theoretical simulations performed with a Monte-Carlo approach. EXAFS and XRPD data provide structural parameters, such as interatomic distances, coordination numbers, cell parameters, concentration of hydride and carbide phases, in the palladium nanocatalysts exposed to different amounts of hydrogen and acetylene.

2. Materials and methods

2.1. Catalyst preparation and activation

We used the 5 wt.% Pd on carbon catalyst D1190 from the Chimet S.p.A. catalyst library (http://www.chimet.com/en/d1190). The sample was prepared using deposition–precipitation method on a wood-based activated carbon [63] (surface area = 980 $m^2\ g^{-1}$; pore volume = 0.62 $cm^3\ g^{-1}$) as extensively described elsewhere [64–66].

Before collecting experimental data, the sample was pretreated in hydrogen at 125 °C *in situ* and then outgassed and cooled down to 100 °C. This procedure guarantees to have a clean metallic phase for the starting material, avoiding the undesired surface oxidized phase observed on Pd nanoparticles exposed to air [66,67]. Experimental EXAFS spectra and XRPD patterns presented in this paper were collected at 100 °C under the following conditions: in vacuum, which corresponds to bare palladium nanoparticles, in 100 and 600 mbar of pure hydrogen, which resulted in hydride formation, in a mixture of 650 mbar of hydrogen and 350 mbar of acetylene, and in 1000 mbar of pure acetylene. Each time before changing the external conditions, the pretreatment procedure was repeated and XRPD data were collected to establish that the structure of the sample corresponds to bare palladium.

2.2. Experimental setup

X-ray absorption and X-ray powder diffraction measurements were performed at the Swiss-Norwegian Beamline (BM01B) of the European Synchrotron Radiation Facility (ESRF), Grenoble, France. The sample was loaded into a glass capillary of 1 mm diameter. The capillary was oriented horizontally and perpendicularly to the X-ray beam. A gas blower was positioned above the sample to control the temperature during the experiment. The capillary was glued into a metal holder connected with a pressurized setup, which allowed remotely controlling gas content and pressure inside the capillary. The minimal pressure, which was reached by using a scroll pump, was less than 0.1 mbar.

Experimental data were collected using different pressures of hydrogen (99.999% purity), acetylene (99.6%) and a mixture of these gasses. Under each of the selected conditions, both X-ray absorption and X-ray powder diffraction measurements were performed. The beamline allows a rapid (about 30 s) plug and play switching between X-ray absorption and X-ray diffraction setups. Pd K-edge EXAFS data were collected in transmission mode using ionization chambers in the energy range of 24.1–25.4 keV employing a double crystal Si(111) monochromator in the continuous scanning mode. A palladium foil was measured simultaneously as a reference compound for energy calibration. After each X-ray absorption scan, 20 diffraction patterns were recorded by the CMOS-Dexela 2D detector. Each pattern was recorded with an acquisition time of 5 s and was followed by a dark scan used for background subtraction. The wavelength of $\lambda = 0.50544(6)$ Å was selected by a channel-cut Si(111) monochromator. The λ and the sample to detector distance, were calibrated using Si and LaB_6 powder NIST standards. The detector size and the chosen sample to detector distance allowed collecting diffraction patterns in a 2θ range between 5 and 52°, corresponding to a 5.79–0.57 Å d-spacing interval.

2.3. Data processing and analysis

EXAFS data were analyzed by means of the Ifeffit package [68], including background removal, normalization, energy shift correction, Fourier transformation, and fitting using theoretical amplitude and phase functions calculated by the FEFF6 code [42]. A first-shell fit of Fourier-transformed data was performed in real space between 1.5 and 3.1 Å utilizing k^2-weighted normalization of $\chi(k)$ in the k-range from 5 to 12 $Å^{-1}$. Such interval of Δk was chosen to reduce the effect of the support [41], as the main contribution of Pd-C bonds occurs below 5 $Å^{-1}$, while at higher k the signal is dominated by Pd-Pd contributions. The number of independent parameters of such fits ($2\Delta k \Delta R/\pi$) results larger than seven. The first shell Pd-Pd interatomic distance ($R_{Pd\text{-}Pd}$), Debye-Waller parameter (σ^2), zero energy shift (ΔE_0) and first shell coordination number (N) were optimized in the fits. The value of the passive electron reduction factor $S_0{}^2 = 0.83$ was obtained by fitting the spectra of the palladium foil model and successively kept as a fixed parameter for the fits performed on the nanostructured sample.

For XANES calculation FEFF8.4 code [42,55] was applied using the Hedin-Lundqvist exchange correlation potential [69]. For the pure metallic phase, XANES calculation were performed on spherical clusters of fcc palladium of increasing size starting from a radius of 3 Å and adding progressively an additional shell of 1 Å. At each step the XANES simulations were compared and the procedure ended when the difference between the two successive steps were negligible. For R = 8 Å convergence was achieved. In the case of palladium hydride and carbide, hydrogen and carbon atoms were incorporated in the octahedral interstitials of the palladium lattice to reach the simulated PdH_x (PdC_y) stoichiometry. For any given stoichiometry, 1000 different microscopic configurations were obtained allowing to move hydrogen (carbon) atoms from

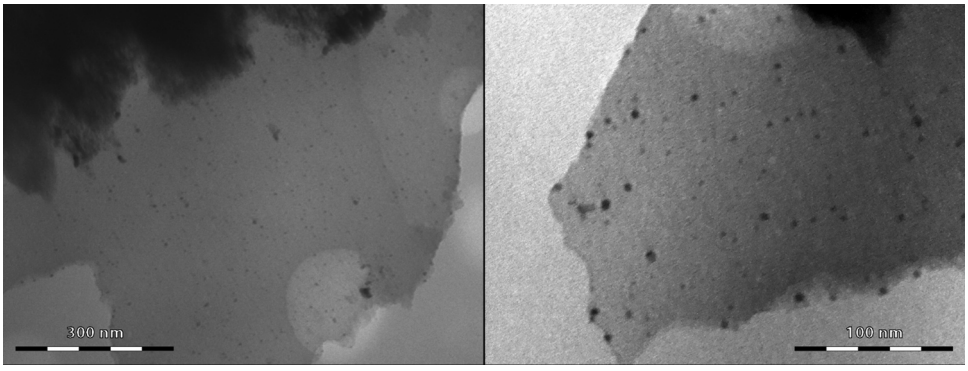

Fig. 1. Representative TEM micrographs for palladium nanoparticles (black dots) deposited on carbon (grey areas).

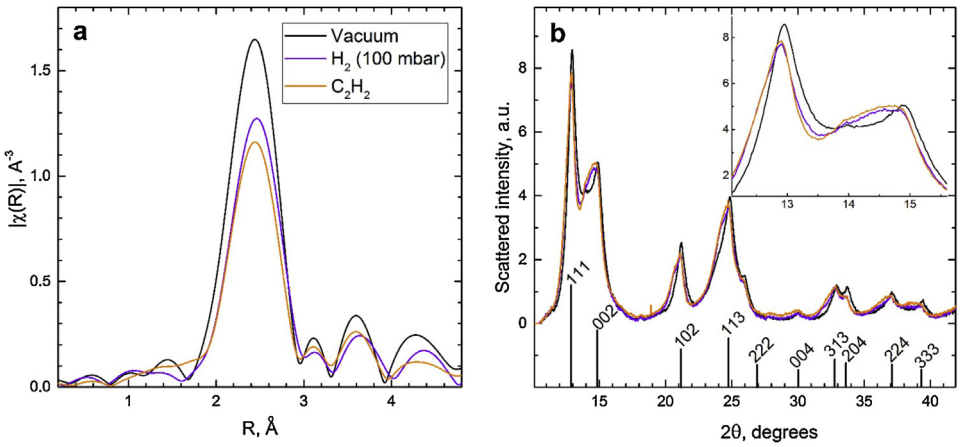

Fig. 2. Magnitude of the k^2-weighted, phase uncorrected, FT of the experimental EXAFS data (a) and background subtracted XRPD patterns (b) collected at 100 °C on the palladium nanoparticles in vacuum (black), and after interaction with 100 mbar of hydrogen (violet), or 1000 mbar of acetylene (orange). Observed reflections of the fcc phase are also reported in part (b). XRPD pattern were collected using λ = 0.50544(6) Å. (For interpretation of the references to colour in this figure legend, the reader is referred to the web version of this article.)

vacancy to vacancy inside the 8 Å palladium cluster by applying a Monte-Carlo approach. Theoretical spectra of palladium hydride and carbide were obtained by calculating and averaging of 1000 spectra corresponding to the microscopic configurations generated by the Monte-Carlo procedure. The FitIt-3 code [70,71] was used for fitting the experimental spectra by theoretical ones to obtain the best stoichiometry x (y) for the given experimental spectrum.

For XRPD data, dark field subtraction, averaging and azimuthal integration of diffraction images were performed by means of PyFAI package [72,73]. Rietveld analysis of the diffraction patterns was carried out in Jana2006 code [74]. The procedure included refinement of profile and background parameters, zero angle shift, cell parameters of two phases and their relative concentrations. The background was simulated using a 10-parameter Chebyshev function, while for the peak profile a 3-parameter pseudo-Voigt function was used.

3. Results and discussion

3.1. Sample characterization

Transmission electron microscopy images (Fig. 1) were collected using Tecnai G2 Spirit Bic TWIN FEI electron microscope operated at 100 kV. According to TEM analysis, the average nanoparticle size was 5.1 ± 0.8 nm. See Fig. S4 of the Supplementary material for the particle size distribution obtained from TEM.

3.2. Determination of hydride and carbide phases

Firstly, the structure of the catalyst exposed separately to a pure hydrogen and pure acetylene was investigated. Fig. 2 shows the FT of the EXAFS spectra (part a) and the XRPD patterns (part b) collected on the as activated catalyst (black curves) compared with those obtained after interaction with 100 mbar of hydrogen (violet curves) and 1000 mbar of acetylene (orange curves). The adopted conditions are known to form palladium hydride [34,59], and carbide [75,76] phases, respectively. The data reported in Fig. 2 indicate that it will be very hard to discriminate between hydride and carbide phases as they result in very similar experimental signals in both Fourier-transform of EXAFS and in XRPD patterns. Indeed, both techniques detect the new phase formation in an indirect way, that is the lattice expansion due to heteroatom insertion inside the fcc framework. This effect is analogous in both cases. When we expose the sample to pure gases, as done in the experiments reported in Fig. 2, we can obviously know in advance if we form hydride or carbide. However, the problem becomes more complex under reaction conditions, when a mixture of hydrogen and acetylene is sent and both hydride and carbide phases have a probability to be formed, since very similar responses are expected to be observed by both EXAFS and XRPD techniques independently on the phase actually formed: PdH_x, PdC_y or PdH_xC_y.

X-ray absorption near-edge structure (XANES) [12,13,42,46,55–58,77–80] allows us to overcome these difficulties and discriminate between palladium hydride and carbide phases. Fig. 3a shows that in the presence of hydrogen (violet

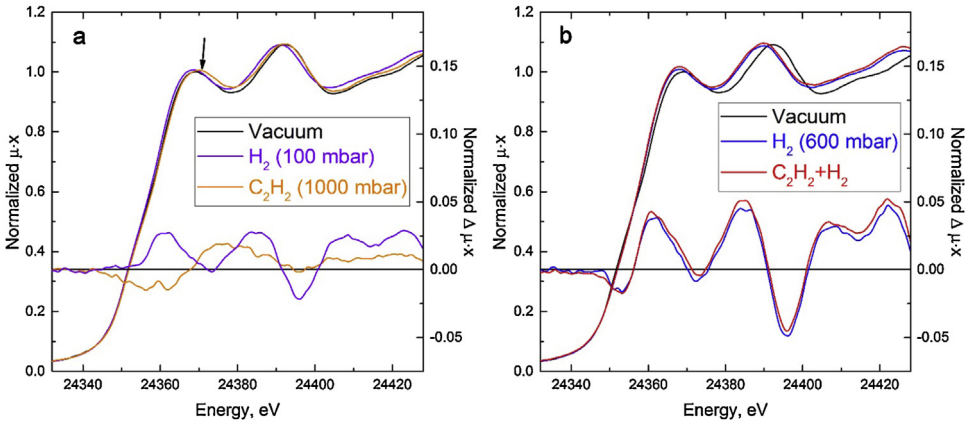

Fig. 3. Part (a): Experimental Pd K-edge XANES spectra (left ordinate axis) and difference XANES (right ordinate axis) collected at 100 °C on the palladium nanoparticles in vacuum (black), in 100 mbar (violet) and in 1000 mbar of acetylene (orange). Part (b), as part (a) for a mixture of 650 mbar of hydrogen and 350 mbar of acetylene (red) and 600 mbar of hydrogen (blue). For comparison the spectrum collected in vacuum conditions is also reported (black). (For interpretation of the references to colour in this figure legend, the reader is referred to the web version of this article.)

Table 1
Structural parameters obtained from the analysis of EXAFS, XRPD and XANES data. First shell EXAFS data analysis provides the average coordination number (N), the Pd-Pd distance ($R_{Pd\text{-}Pd}$), the Debye-Waller factor (σ^2) and the ionization energy (E_0). The $S_0{}^2$ factor was fixed to the value 0.83 obtained by fitting the EXAFS spectrum of Pd foil (N = 12). The Rietveld refinement of XRPD allows to obtain: (i) the fractions of pure Pd metal ($1-X_{H,C}$) and of the hydride or carbide phase ($X_{H,C}$) and (2) the lattice parameter of the hydride or carbide phase ($a_{PdH,C}$), being the lattice parameter of the pure metal phase fixed to the value obtained on the just reduced sample (a_{Pd} = 3.88 Å). Comparison with the EXAFS results is obtained reporting the average lattice parameter $\langle a\rangle = (1-X_{H,C})\,a_{Pd} + X_{H,C}\,a_{PdH,C}$ and using the geometrical relationship in fcc lattices: $R_{Pd\text{-}Pd} = \langle a\rangle/\sqrt{2}$. The last column reports the stoichiometry of the hydride (or carbide) phase as determined from Monte Carlo simulation of the XANES spectra. Values reported without error bars are non-optimized parameters that have been fixed during the fitting procedure. Note that in the bulk Pd metal a = 3.8907 Å and $R_{Pd\text{-}Pd}$ = 2.7511 Å.

Pressure (mbar)	Gas	EXAFS				XRPD				XANES
		N	$R_{Pd\text{-}Pd}$ (Å)	σ^2 (Å^2)	E_0 (eV)	$X_{H,C}$	$a_{PdH,C}$	$\langle a\rangle$ (Å)	$R_{Pd\text{-}Pd}$ (Å)	PdH_x/PdC_y
0	–	9.4(4)	2.74(1)	0.007(1)	24357.5(8)	0	–	3.88(1)	2.744(7)	–
100	H_2	9.4	2.77(1)	0.008(1)	24356.7(9)	0.55(9)	3.95(1)	3.92(1)	2.772(7)	$PdH_{0.20(5)}$
600	H_2	9.4	2.82(1)	0.008(1)	24357.1(9)	1.00	4.00(1)	4.00(1)	2.828(7)	$PdH_{0.30(5)}$
1000	C_2H_2	9.4	2.76(1)	0.009(1)	24357.3(9)	0.62(9)	3.96(1)	3.93(1)	2.779(7)	$PdC_{0.13(5)}$
650 + 350	$H_2 + C_2H_2$	9.4	2.81(1)	0.008(1)	24356.9(9)	1.00	4.00(1)	4.00(1)	2.828(7)	$PdH_{0.30(5)}$

curve) the first near-edge peak at 24369 eV becomes narrower and is shifted by 1 eV to lower energy. Formation of palladium carbide (orange curve) leads to a broadening of the same peak and shifts it by 1 eV to higher energy. This opposite behavior of XANES spectra during hydride and carbide formation is more pronounced in the difference spectra [81] and provides us a method to discriminate between the two phases under hydrogenation reaction conditions. To test this thesis we investigated the system sending at 100 °C a mixture of 650 mbar of hydrogen and 350 mbar of acetylene, see red curve in Fig. 3b. Comparing the XANES spectrum collected under hydrogenation reaction conditions with those obtained sending at 100 °C the pure reagents separately (100 and 600 mbar of H_2 or 1000 mbar of C_2H_2) we can conclude that hydride phase is formed, having a similar composition to that obtained sending 600 mbar of pure hydrogen at the same temperature.

3.3. Theoretical simulation of XANES

Calculation of XANES spectra for palladium hydride and carbide structures was performed applying Monte-Carlo simulation of hydrogen and carbon atoms occupancy in the octahedral interstitials of the palladium lattice. For each of the selected concentrations x and y of PdH_x and PdC_y respectively, we have generated 1000 different geometries and have used them for XANES simulation. The resulting spectra were averaged and used for quantitative fitting of experimental XANES. Fig. 4a shows the evolution of the difference XANES spectra for the PdH_x phase in the $0 \le x \le 0.5$ range. Part (b) of the same figure reports the analogous theoretical difference XANES spectra for the PdC_y phase in the $0 \le y \le 0.2$ interval.

Comparing the theoretical difference XANES spectra reported in Fig. 4a,b with the experimental ones reported in Fig. 3a, it becomes evident that the simulation of the XANES spectra is not just allowing to discriminate between PdH_x and PdC_y phases, but can be used also to quantitatively determine the stoichiometry of the phase formed in a given experimental condition, fitting the best x (y) value to better reproduce the experimental spectrum.

The fitting procedure was performed using a multidimensional interpolation approach implemented in the FitIt-3 code [70,71]. A minimization of the root-mean-square difference between experimental and theoretical spectra in the region from 24350 to 24410 eV was used for structural refinement. For both hydrogen and carbon interstitial defects we have calculated series of spectra on a two dimensional grid of parameters: concentration of defects and Pd-Pd distances. Calculated spectra, corresponding to different concentrations of hydrogen and carbon, and different interatomic distances, were used subsequently as interpolation nodes. Spectra of any required intermediate concentrations and interatomic distance were predicted based on the interpolation approach. The quantitative hydrogen and carbon concentrations were refined for each spectrum, while interatomic distances were fixed according to EXAFS analysis results (see Table 1). In particular, the resulting concentration of x hydrogen atoms in the sample exposed to 600 mbar of hydrogen converged to a value of $x = 0.30 \pm 0.05$ ($PdH_{0.3}$). The concentration of carbon in the acetylene-exposed sample was found to be $y = 0.13 \pm 0.05$ ($PdC_{0.13}$). The error values correspond to a maximal change in the x or y parameters which results in the change of Fit Index [71] for the difference spectra smaller than 10^{-3}. The XANES spectra of the simulations of the

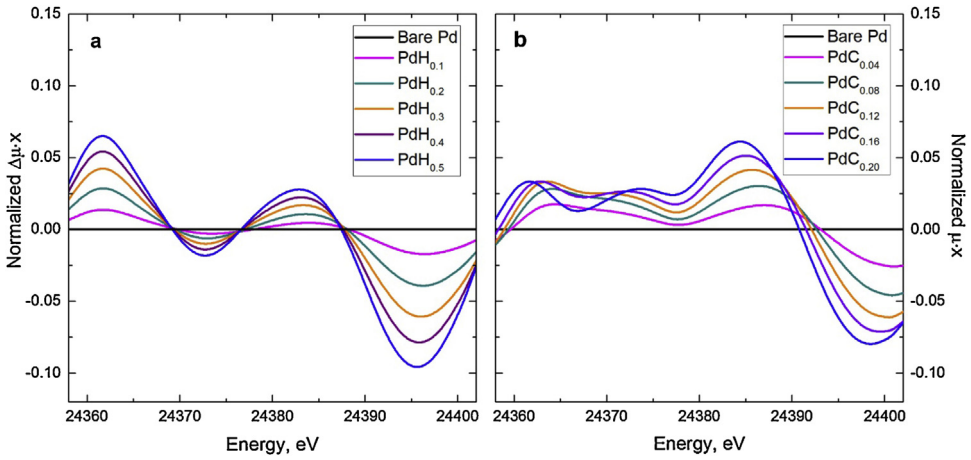

Fig. 4. Part (a): Theoretical Pd K-edge difference XANES spectra for the PdH_x phase in the $0 \le x \le 0.5$ stoichiometry interval. Part (b): as part (a) for the PdC_y phase in the $0 \le y \le 0.2$ stoichiometry interval.

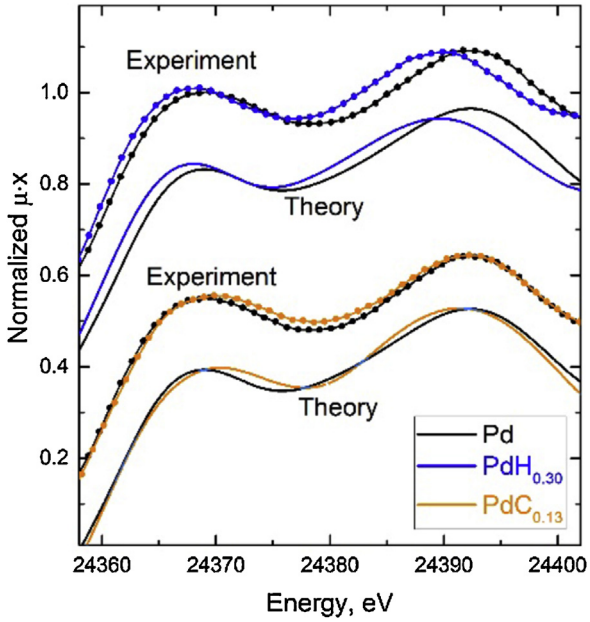

Fig. 5. Experimental (lines with circles) and theoretical (solid lines) Pd K-edge XANES spectra. Black, blue and orange curves correspond to bare metal, hydride and carbide phases respectively. For better visualization, spectra are shifted in vertical direction. (For interpretation of the references to colour in this figure legend, the reader is referred to the web version of this article.)

$PdH_{0.30}$ and $PdC_{0.13}$ are reported in Fig. 5, together with the experimental curves. To appreciate the modification undergone by the XANES spectrum upon H (C) atoms intercalation, the spectra (simulated and experimental) of pure Pd metal phase (black curves) are also reported.

3.4. EXAFS and XRPD analysis

The quality of the first shell EXAFS data analysis can be appreciated in Fig. 6, while the quantitative results are summarized in Table 1. First shell analysis of the reduced sample (first row in Table 1) results in a Pd-Pd interatomic distance ($R_{Pd\text{-}Pd}$) of 2.74 ± 0.01 Å and to a coordination number $N = 9.4 \pm 0.4$. As expected these values are smaller with respect to the bulk values: $R_{Pd\text{-}Pd} = 2.7511$ Å and $N = 12$ [82–89]. EXAFS analysis also indicated that in case of palladium hydride the Pd-Pd interatomic distance increases from 2.74 ± 0.01 Å to 2.77 ± 0.01 Å and 2.82 ± 0.01 Å for hydrogen pressures of 100 and 600 mbar respectively (Table 1). Sending a mixture of acetylene and hydrogen leads to the increase of interatomic distance to 2.81 ± 0.01 Å. Finally, exposure to pure acetylene caused an increase to 2.76 ± 0.01 Å. The carbide phase, formed after exposure to acetylene, was stable and did not decompose after thermal treatment in hydrogen. Changes in coordination number for different spectra were smaller than the error. Thus, the final fit was performed simultaneously for all spectra with common coordination number, resulting in the value $N = 9.4 \pm 0.4$.

The Debye-Waller parameter (σ^2) increased from 0.007 Å^2 for bare nanoparticles to 0.008–0.009 Å^2 in the presence of gases. The increase of Debye-Waller parameter in hydride phase is explained by the fact that palladium hydride phase formation is size dependent [19]. Thus, having the distribution of particle size [89], we obtain the distribution of interatomic distances at given temperature and hydrogen pressure.

For PdC_y obtained in pure acetylene, the increase of the average interatomic distance is 0.02 Å, which is the result of coexisting bare palladium and newly forming carbide phase. In general, problems in resolving local atomic-structure distortions often occur

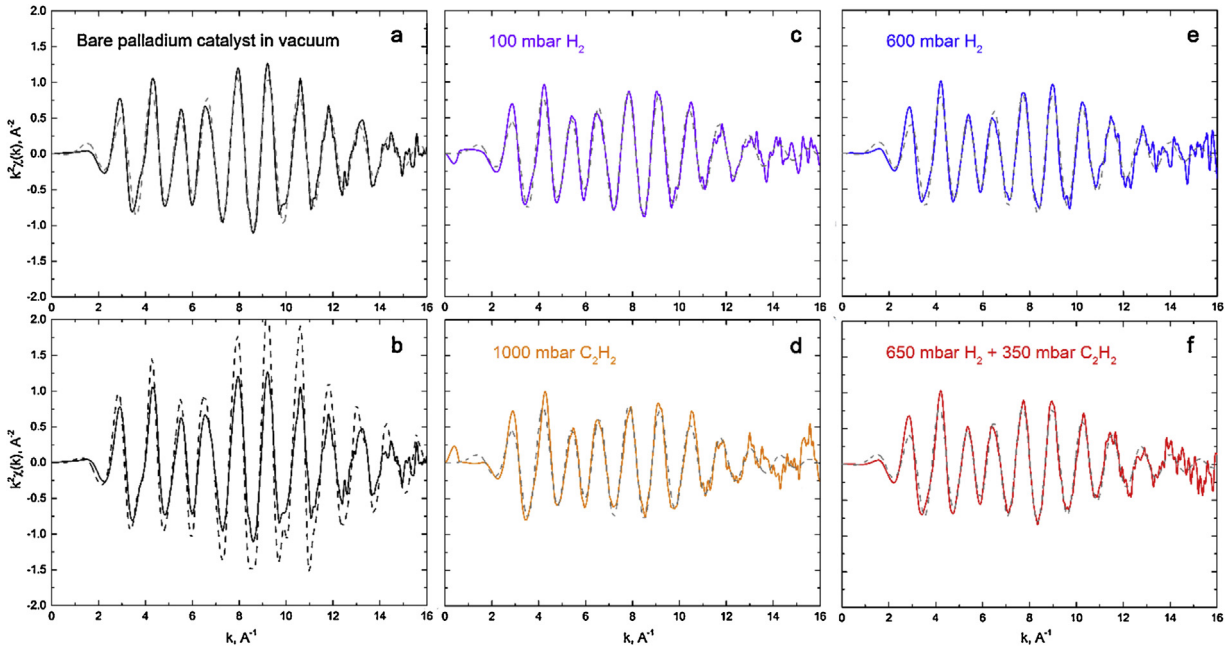

Fig. 6. a, c–f: Experimental (solid curves) and corresponding best fit (dashed gray curves) k^2-weighted EXAFS curves. b: Comparison between Pd nanoparticle (solid curve) and Pd bulk reference material (dashed curve).

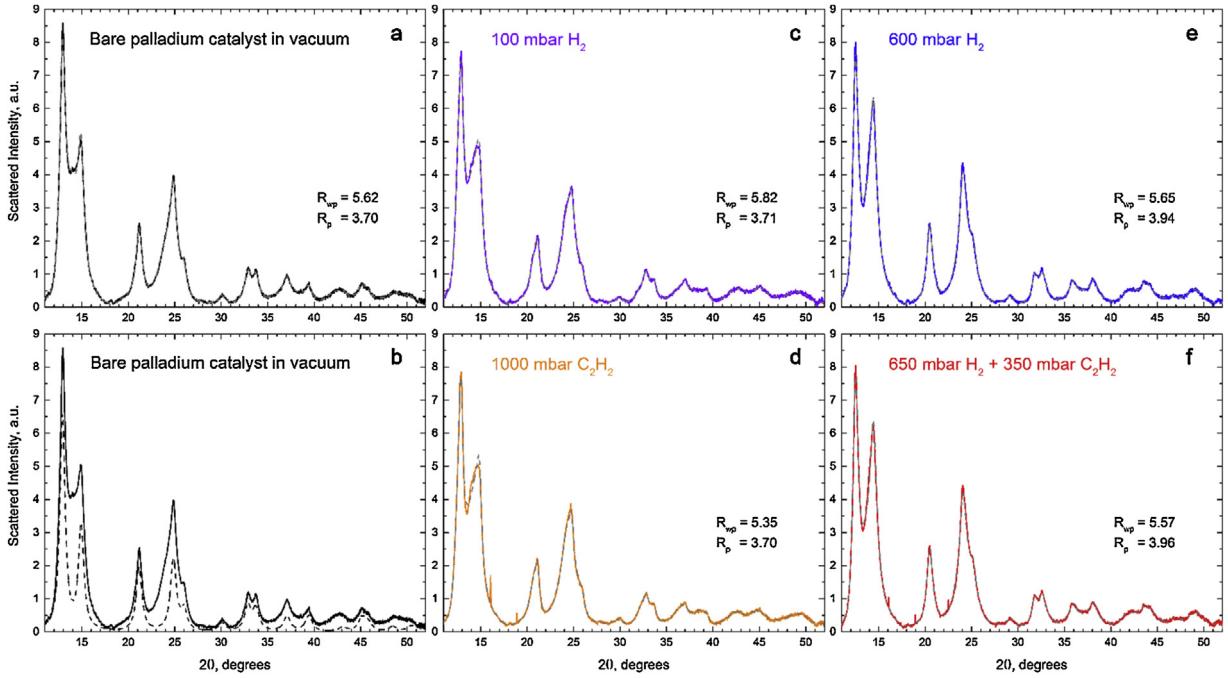

Fig. 7. a, c–f: Experimental (solid curves) and theoretical (obtained from Rietveld refinement, dashed gray curves) X-ray diffraction patterns (λ = 0.50544(6) Å) with corresponding R_{wp} and R_p values. b: Initial (solid) and background subtracted (dashed) experimental patterns. Large background level around 2θ 14° and 24° is a contribution of scattering from the carbon support.

for changes than 0.1 Å [90]. This means that although the relative changes in the average Pd-Pd distance can be resolved with standard EXAFS resolution of 0.01 Å, the coexistence of two distances in one sample cannot be resolved due to high (>0.9) correlation between σ^2 and ΔR (difference between two interatomic distances).

Analysis of XRPD data indicates similar behavior of the palladium nanocatalyst as is observed in X-ray absorption spectra. To obtain structural parameters we have performed Rietveld for the XRPD data in 2θ range from 10 to 50 (see Fig. 7), which contains 13 palladium reflections with a sufficiently high intensity for quantitative treatment: see Fig. 2b for the indexing the 10 reflection in the 10–40° 2θ interval. The profile parameters, zero shift and background were refined using the pattern of bare Pd and fixed for the other patterns. Two phases were used to refine the patterns of palladium hydride and carbide (first phase corresponds to bare palladium, second–to hydride or carbide respectively). The cell parameters of each phase and relative phase concentration were used as fitting parameters.

The advantage of XRPD is that the technique is phase-selective and gives detailed information in the case when several phases coexist in one sample. In contrast to EXAFS, the obtained atomic isotropic displacement parameter of palladium was equal to 0.006 and did not change considerably for different patterns. After exposure to pure acetylene, and 100 mbar of pure hydrogen a new phase started to appear, at the positions with slightly smaller 2θ angles than the initials peaks of bare palladium. It gives a clear understanding that there is the coexistence of two phases, which also explains the Debye-Waller increase obtained from EXAFS. The peaks, which appeared after exposure to acetylene and correspond to palladium carbide did not disappear after removal of acetylene and heating to 125 °C in hydrogen.

Table 1 also compares the structural parameters obtained from EXAFS and XRPD. As was discussed above, after exposure to 100 mbar H_2 or 1000 mbar C_2H_2, the hydride or carbide phases coexist with pure palladium phase. For these patterns, the double phase refinement was performed, the averaged cell parameter a was calculated as a weighted sum of cell parameters of these phases and the concentration of the second phase (hydride or carbide) $X_{H,C}$ is reported. We should note that high correlation between phase concentration and Δa difference between the cell parameters of different phases results in bigger error in determining this parameters. However, the value of the averaged cell parameter was examined to be stable. The patterns for which the phase concentrations do not report the error bar were refined using only one phase.

The comparison between the average $R_{Pd\text{-}Pd}$ obtained from the EXAFS data analysis and the equivalent value obtained from XRPD refinement ($R_{Pd\text{-}Pd} = \langle a \rangle/\sqrt{2}$, where $\langle a \rangle = (1 - X_{H,C})\, a_{Pd} + X_{H,C}\, a_{PdH,C}$) resulted in a perfect agreement, within the corresponding error bars, see Table 1.

A more precise structural determination of PdC or PdH nanoparticles can, in principle, be obtained with a full profile analysis of the diffuse scattering [91–94], going beyond the Bragg-peak analysis performed in the presented Rietveld refinements. In the present case this more sophisticated analysis is however of difficult application as most of the diffuse scattering comes from the carbon support, that represents 95 wt.% of the material contributing to the scattering.

4. Conclusions

We have set a strategy to obtain structural information on supported palladium nano-particles relevant in catalysis by applying *in situ* and *operando* X-ray absorption and powder diffraction techniques. Analysis of XANES spectra allows determining whether hydride or carbide phase is formed in the nano-particles. Possibility to extract this information from XANES becomes extremely important in some cases, when the catalyst is exposed to a mixture of gasses, and the type of the phase (carbide or hydride) cannot be predicted in advance. In addition to the type of the phase determined from XANES, and interatomic distance obtained from EXAFS, XRPD analysis gives quantitative information on the phase concentrations.

The described scheme of experimental measurements and analysis may be applied to investigate the structural evolution of supported metal nano particle catalyst during catalytic processes in *operando* conditions, such as hydrogenation of hydrocarbons and will allow correlating catalytic properties of the nanoparticles with their structure and phase content.

Acknowledgments

A.L.B., A.A.G., K.A.L., A.V.S. and C.L. acknowledge mega-grant of Ministry of Education and Science of the Russian Federation (14.Y26.31.0001) for funding the research. A.L.B. and A.A.G. acknowledge the Grant of the President of Russia for Young ScientistsMK-3206.2014.2. K.A.L. acknowledges the scholarship of the President of Russia for PhD students and young scientists no. СП-2796.2016.1

Appendix A. Supplementary data

Supplementary data associated with this article can be found, in the online version, at http://dx.doi.org/10.1016/j.cattod.2016.02.065.

References

[1] R.M. Crooks, M.Q. Zhao, L. Sun, V. Chechik, L.K. Yeung, Acc. Chem. Res. 34 (2001) 181.
[2] M. Moreno-Manas, R. Pleixats, Acc. Chem. Res. 36 (2003) 638.
[3] S. Eustis, M.A. El-Sayed, Chem. Soc. Rev. 35 (2006) 209.
[4] M.A. Newton, Chem. Soc. Rev. 37 (2008) 2644.
[5] J.M. Campelo, D. Luna, R. Luque, J.M. Marinas, A.A. Romero, ChemSusChem 2 (2009) 18.
[6] R.J. White, R. Luque, V.L. Budarin, J.H. Clark, D.J. Macquarrie, Chem. Soc. Rev. 38 (2009) 481.
[7] J. Dupont, J.D. Scholten, Chem. Soc. Rev. 39 (2010) 1780.
[8] S. Shylesh, V. Schunemann, W.R. Thiel, Angew. Chem. Int. Ed. 49 (2010) 3428.
[9] J. Singh, C. Lamberti, J.A. van Bokhoven, Chem. Soc. Rev. 39 (2010) 4754.
[10] A. Dhakshinamoorthy, H. Garcia, Chem. Soc. Rev. 41 (2012) 5262.
[11] X.H. Li, M. Antonietti, Chem. Soc. Rev. 42 (2013) 6593.
[12] L. Mino, G. Agostini, E. Borfecchia, D. Gianolio, A. Piovano, E. Gallo, C. Lamberti, J. Phys. D: Appl. Phys. 46 (2013) 423001.
[13] S. Bordiga, E. Groppo, G. Agostini, J.A. van Bokhoven, C. Lamberti, Chem. Rev. 113 (2013) 1736.
[14] D. Teschner, J. Borsodi, A. Wootsch, Z. Revay, M. Havecker, A. Knop-Gericke, S.D. Jackson, R. Schlögl, Science 320 (2008) 86.
[15] D. Teschner, J. Borsodi, Z. Kis, L. Szentmikloísi, Z. Reívay, A. Knop-Gericke, R. Schlögl, D. Torres, P. Sautet, J. Phys. Chem. C 114 (2010) 2293.
[16] F.A. Lewis, Platinum Met. Rev. 26 (1982) 20.
[17] F.D. Manchester, A. San-Martin, J.M. Pitre, J. Phase Equilib. 15 (1994) 62.
[18] V.P. Zhdanov, B. Kasemo, Chem. Phys. Lett. 460 (2008) 158.
[19] C. Langhammer, V.P. Zhdanov, I. Zorić, B. Kasemo, Chem. Phys. Lett. 488 (2010) 62.
[20] A.L. Bugaev, V.V. Srabionyan, A.V. Soldatov, L.A. Bugaev, J.A. van Bokhoven, J. Phys. Conf. Ser. 430 (2013) 012028.
[21] H. Jobic, A. Renouprez, J. Less Common Met. 129 (1987) 311.
[22] R. Davis, S. Landry, J. Horsley, M. Boudart, Phys. Rev. B 39 (1989) 10580.
[23] T.B. Flanagan, W.A. Oates, Annu. Rev. Mater. Sci. 21 (1991) 269.
[24] J.A. McCaulley, J. Phys. Chem. 97 (1993) 10372.
[25] A. Soldatov, S. Della Longa, A. Bianconi, Solid State Commun. 85 (1993) 863.
[26] F.A. Lewis, Int. J. Hydrogen Energy 20 (1995) 587.
[27] A. Borodziński, Catal. Lett. 71 (2001) 169.
[28] N.K. Nag, J. Phys. Chem. B 105 (2001) 5945.
[29] T. Mitsui, M.K. Rose, E. Fomin, D.F. Ogletree, M. Salmeron, Nature 422 (2003) 705.
[30] S. Kishore, J. Nelson, J. Adair, P. Eklund, J. Alloys Compd. 389 (2005) 234.
[31] M. Yamauchi, R. Ikeda, H. Kitagawa, M. Takata, J. Phys. Chem. C 112 (2008) 3294.
[32] A. Shabaev, D.A. Papaconstantopoulos, M.J. Mehl, N. Bernstein, Phys. Rev. B 81 (2010), 184103.
[33] T. Shegai, C. Langhammer, Adv. Mater. 23 (2011) 4409.
[34] A.L. Bugaev, A.A. Guda, K.A. Lomachenko, V.V. Srabionyan, L.A. Bugaev, A.V. Soldatov, C. Lamberti, V.P. Dmitriev, J.A. van Bokhoven, J. Phys. Chem. C 118 (2014) 10416.
[35] M.W. Tew, M. Janousch, T. Huthwelker, J.A. van Bokhoven, J. Catal. 283 (2011) 45.
[36] M.W. Tew, M. Nachtegaal, M. Janousch, T. Huthwelker, J.A. van Bokhoven, Phys. Chem. Chem. Phys. 14 (2012) 5761.
[37] M. Suleiman, N. Jisrawi, O. Dankert, M. Reetz, C. Bähtz, R. Kirchheim, A. Pundt, J. Alloys Compd. 356 (2003) 644.
[38] W. Vogel, W. He, Q.-H. Huang, Z. Zou, X.-G. Zhang, H. Yang, Int. J. Hydrogen Energy 35 (2010) 8609.
[39] Z.A. Chase, J.L. Fulton, D.M. Camaioni, D. Mei, M. Balasubramanian, V.-T. Pham, C. Zhao, R.S. Weber, Y. Wang, J.A. Lercher, J. Phys. Chem. C 117 (2013) 17603.
[40] D. Scarano, S. Bordiga, C. Lamberti, G. Ricchiardi, S. Bertarione, G. Spoto, Appl. Catal. A 307 (2006) 3.
[41] V.V. Srabionyan, A.L. Bugaev, V.V. Pryadchenko, L.A. Avakyan, J.A. van Bokhoven, L.A. Bugaev, J. Phys. Chem. Solids 75 (2014) 470.

[42] J.J. Rehr, R.C. Albers, Rev. Mod. Phys. 72 (2000) 621.
[43] C. Lamberti, Surf. Sci. Rep. 53 (2004) 1.
[44] S. Bordiga, F. Bonino, K.P. Lillerud, C. Lamberti, Chem. Soc. Rev. 39 (2010) 4885.
[45] C. Garino, E. Borfecchia, R. Gobetto, J.A. van Bokhoven, C. Lamberti, Coord. Chem. Rev. 277 (2014) 130.
[46] J.A. van Bokhoven, C. Lamberti, Coord. Chem. Rev. 277 (2014) 275.
[47] S.G. Fiddy, J. Evans, M.A. Newton, T. Neisius, R.P. Tooze, R. Oldman, Chem. Commun. (2003) 2682.
[48] A. Iglesias-Juez, A. Martinez-Arias, M.A. Newton, S.G. Fiddy, M. Fernandez-Garcia, Chem. Commun. (2005) 4092.
[49] M.A. Newton, C. Belver-Coldeira, A. Martinez-Arias, M. Fernandez-Garcia, Nat. Mater. 6 (2007) 528.
[50] A. Kubacka, A. Martinez-Arias, M. Fernandez-Garcia, M.A. Newton, Catal. Today 145 (2009) 288.
[51] A.F. Lee, C.V. Ellis, J.N. Naughton, M.A. Newton, C.M.A. Parlett, K. Wilson, J. Am. Chem. Soc. 133 (2011) 5724.
[52] D. Ferri, M.S. Kumar, R. Wirz, A. Eyssler, O. Korsak, P. Hug, A. Weidenkaff, M.A. Newton, Phys. Chem. Chem. Phys. 12 (2010) 5634.
[53] A. Iglesias-Juez, A. Kubacka, M. Fernandez-Garcia, M. Di Michiel, M.A. Newton, J. Am. Chem. Soc. 133 (2011) 4484.
[54] D. Narehood, S. Kishore, H. Goto, J. Adair, J. Nelson, H. Gutierrez, P. Eklund, Int. J. Hydrogen Energy 34 (2009) 952.
[55] J.J. Rehr, A.L. Ankudinov, Coord. Chem. Rev. 249 (2005) 131.
[56] A. Bianconi, J. Garcia, M. Benfatto, Top. Curr. Chem. 145 (1988) 29.
[57] M. Fernandez-Garcia, Catal. Rev. Sci. Eng. 44 (2002) 59.
[58] S.A. Guda, A.A. Guda, M.A. Soldatov, K.A. Lomachenko, A.L. Bugaev, C. Lamberti, W. Gawelda, C. Bressler, G. Smolentsev, A.V. Soldatov, Y. Joly, J. Chem. Theory Comput. 11 (2015) 4512.
[59] M.W. Tew, J.T. Miller, J.A. van Bokhoven, J. Phys. Chem. C 113 (2009) 15140.
[60] A.L. Bugaev, A.A. Guda, K.A. Lomachenko, L.A. Bugaev, A.V. Soldatov, Bull. Russ. Acad. Sci. Phys. 79 (2015) 1180.
[61] P. D'Angelo, M. Benfatto, S. Della Longa, N.V. Pavel, Phys. Rev. B 66 (2002), 064209.
[62] C.P. Balde, A.E. Mijovilovich, D.C. Koningsberger, A.M.J. van der Eerden, A.D. Smith, K.P. de Jong, J.H. Bitter, J. Phys. Chem. C 111 (2007) 11721.
[63] A. Piovano, A. Lazzarini, R. Pellegrini, G. Leofanti, G. Agostini, S. Rudić, A.L. Bugaev, C. Lamberti, E. Groppo, Adv. Condens. Matter Phys. (2015) 803267.
[64] R. Pellegrini, G. Leofanti, G. Agostini, E. Groppo, M. Rivallan, C. Lamberti, Langmuir 25 (2009) 6476.
[65] G. Agostini, E. Groppo, A. Piovano, R. Pellegrini, G. Leofanti, C. Lamberti, Langmuir 26 (2010) 11204.
[66] G. Agostini, C. Lamberti, R. Pellegrini, G. Leofanti, F. Giannici, A. Longo, E. Groppo, ACS Catal. 4 (2014) 187.
[67] E. Groppo, G. Agostini, A. Piovano, N.B. Muddada, G. Leofanti, R. Pellegrini, G. Portale, A. Longo, C. Lamberti, J. Catal. 287 (2012) 44.
[68] B. Ravel, M. Newville, J. Synchrotron Radiat. 12 (2005) 537.
[69] L. Hedin, B.I. Lundqvist, J. Phys. C 4 (1971) 2064.
[70] G. Smolentsev, A. Soldatov, J. Synchrotron Radiat. 13 (2005) 19.
[71] G. Smolentsev, A.V. Soldatov, Comp. Mater. Sci. 39 (2007) 569.
[72] J. Kieffer, D. Karkoulis, J. Phys. Conf. Ser. 425 (2013) 202012.
[73] G. Ashiotis, A. Deschildre, Z. Nawaz, J.P. Wright, D. Karkoulis, F.E. Picca, J. Kieffer, J. Appl. Crystallogr. 48 (2015) 510.
[74] V. Petříček, M. Dušek, L. Palatinus, Z. Kristallogr. 229 (2014) 345.
[75] A.J. Forman, J.N. Park, W. Tang, Y.S. Hu, G.D. Stucky, E.W. McFarland, ChemCatChem 2 (2010) 1318.
[76] M. Crespo-Quesada, S. Yoon, M.S. Jin, Y.N. Xia, A. Weidenkaff, L. Kiwi-Minsker, ChemCatChem 6 (2014) 767.
[77] A.L. Ankudinov, B. Ravel, J.J. Rehr, S.D. Conradson, Phys. Rev. B 58 (1998) 7565.
[78] M. Benfatto, S. Della Longa, J. Synchrot. Radiat. 8 (2001) 1087.
[79] M. Benfatto, S. Della Longa, C.R. Natoli, J. Synchrot. Radiat. 10 (2003) 51.
[80] Y. Joly, Phys. Rev. B 63 (2001) 10.
[81] D.E. Ramaker, D.C. Koningsberger, Phys. Chem. Chem. Phys. 12 (2010) 5514.
[82] A. Balerna, E. Bernieri, P. Picozzi, A. Reale, S. Santucci, E. Burattini, S. Mobilio, Phys. Rev. B 31 (1985) 5058.
[83] A.I. Frenkel, C.W. Hills, R.G. Nuzzo, J. Phys. Chem. B 105 (2001) 12689.
[84] A.I. Frenkel, S. Nemzer, I. Pister, L. Soussan, T. Harris, Y. Sun, M.H. Rafailovich, J. Chem. Phys. 123 (2005) 6.
[85] J.T. Miller, A.J. Kropf, Y. Zha, J.R. Regalbuto, L. Delannoy, C. Louis, E. Bus, J.A. van Bokhoven, J. Catal. 240 (2006) 222.
[86] Y. Sun, A.I. Frenkel, R. Isseroff, C. Shonbrun, M. Forman, K.W. Shin, T. Koga, H. White, L.H. Zhang, Y.M. Zhu, M.H. Rafailovich, J.C. Sokolov, Langmuir 22 (2006) 807.
[87] G. Agostini, S. Usseglio, E. Groppo, M.J. Uddin, C. Prestipino, S. Bordiga, A. Zecchina, P.L. Solari, C. Lamberti, Chem. Mater. 21 (2009) 1343.
[88] G. Agostini, R. Pellegrini, G. Leofanti, L. Bertinetti, S. Bertarione, E. Groppo, A. Zecchina, C. Lamberti, J. Phys. Chem. C 113 (2009) 10485.
[89] G. Agostini, A. Piovano, L. Bertinetti, R. Pellegrini, G. Leofanti, E. Groppo, C. Lamberti, J. Phys. Chem. C 118 (2014) 4085.
[90] L.A. Bugaev, L.A. Avakyan, V.V. Srabionyan, A.L. Bugaev, Phys Rev. B 82 (2010) 064204.
[91] S.J.L. Billinge, I. Levin, Science 316 (2007) 561.
[92] E.S. Božin, P. Juhás, S.J.L. Billinge, Chapter 6—local structure of bulk and nanocrystalline semiconductors using total scattering methods, in: C. Lamberti, G. Agostini (Eds.), Characterization of Semiconductor Heterostructures and Nanostructures, second edition, Elsevier, Oxford, 2013, p. 229.
[93] C. Lamberti, E. Borfecchia, J.A. van Bokhoven, M. Fernández-García, XAS spectroscopy: related techniques and combination with other spectroscopic and scattering methods, in: J.A. van Bokhoven, C. Lamberti (Eds.), X-Ray Absorption and X-Ray Emission Spectroscopy: Theory and Applications, John Wiley & Sons, Chichester, UK, 2016, p. 303.
[94] T.R. Welberry, T. Weber, Crystallogr. Rev 22 (2016) 2.